ORIGINAL RESEARCH ARTICLE

Improving the Interparticle Bonding and Ductility of Cold Sprayed Aluminum Alloys by Deformation Processing

ÖZÜM ÖZSAYGILI, HUANG HUANG, and TEIICHI ANDO

Cold spray (CS) can produce thick coatings and free-standing bulk materials and is adaptable to additive manufacturing, including on-site repair. However, the structural applications of CS materials have been limited by the inherently incomplete interparticle metallurgical bonding in CS materials. In this work, an ultrasonic washing test (UWT) was used to semi-quantitatively assess the extent of interparticle bonding in CS Al6061 and CS Al2024 in relation to key CS parameters and post-CS deformation processing. Results indicate that spraying with a lighter gas or a softer powder promotes the interparticle bonding, although full metallurgical bonding is hardly achieved even by spraying at high deposition efficiencies. Sprayed particles remain in the deposit only because they acquire partial bonding that is sufficient to prevent them from bouncing off. Post-CS rolling and T6 heat treatment increase the interparticle bonding and hence ductility of CS Al alloys. Ultrasonic ironing (UI), a new post-CS deformation processing technique, also produces similar effects. The increased interparticle bonding by post-CS deformation processing arise from fragmentation of oxide layers inherited from powder particle surfaces and consequent metal-to-metal joining at the particle boundaries.

https://doi.org/10.1007/s11661-023-07109-6

I. INTRODUCTION

COLD Spray (CS) is a novel spray deposition process in which solid powder particles, accelerated to velocities up to 1400 m/s in a heated gas stream,[1–4] are deposited onto a substrate to create coatings of metals, polymers, ceramics and composite materials on the substrate.[4–13] Being free from the limitations in conventional thermal spray processes such as oxidation, evaporation, structural degradation, residual stress and gas release, CS provides a unique deposition process for a yet wider spectrum of materials, including reactive and high-temperature sensitive materials.[14]

CS can also produce dense bulk deposits, an ability that potentially makes CS adaptable to additive manufacturing of structural parts, including on-site repair.[15–23] CS is also a severe plastic deformation (SPD) process by which materials with refined microstructures suitable for critical structural applications may be processed.[24–27]

Despite the extensive R&D efforts on CS, however, utilization of CS materials in structural applications is still hampered by their relatively low ductility when compared to their wrought counterparts.[1] The low ductility of CS materials is caused mainly by a lack of complete metallurgical bonding among the deposited particles.[2,7,28–32] Although the relations between the deposition efficiency and CS parameters, *e.g.*, impact velocity and temperature, have been extensively studied and well established,[2,6,33] the extent of metallurgical bonding of deposited particles may have been overlooked as a high deposition efficiency may not necessarily translate into a high degree of interparticle metallurgical bonding.

The motivation of this study was to promote the use of CS materials, particularly CS Al alloys, in structural applications by (1) characterizing the interparticle bonding in relation to process parameters such as spraying gas, *i.e.*, impact velocity, and powder hardness, (2) applying post-CS deformation processing to improve the interparticle bonding and ductility of CS Al alloys and (3) understanding the occurrence of metallurgical bonding in as-sprayed and deformation-processed CS Al materials by transmission electron microscopy (TEM) and scanning transmission electron microscopy (STEM).

ÖZÜM ÖZSAYGILI and TEIICHI ANDO are with the Department of Mechanical and Industrial Engineering, Northeastern University, Boston, MA 02115. Contact e-mail: tando@coe.neu.edu HUANG HUANG is with the Allegro MicroSystems, Manchester, NH 03103.

Manuscript submitted November 10, 2022; accepted June 6, 2023. Article published online June 17, 2023

Table I. CS Conditions of CS Al6061 and Al2024 Samples

Specimen	Al6061-N_2	Al6061-He	Al2024-He
Spraying Gas	nitrogen	helium	helium
Average Impact Velocity	721 m/s	1075 m/s	1050 m/s
Critical Velocity	650 m/s	650 m/s	775 m/s
Gas Temperature	425 °C (698 K)	425 °C (698 K)	425 °C (698 K)

T6 Al6061 substrate for all specimens. The gun-substrate distance was 25 mm for all experiments.

II. EXPERIMENTAL PROCEDURE

A. *Specimen Preparation*

Al2024 and Al6061, chosen as the alloys for this study, are among the most widely used heat treatable aluminum alloys suitable for critical structural parts. They are also studied extensively as CS Al alloys.[24,28] − 325/ + 400 sieved gas-atomized Al2024 and Al6061 powders with mean particle sizes of 35 and 30 μm, respectively, both from Valimet, Inc., were cold-sprayed on Al6061 substrate to prepare strip-shaped Al2024 and Al6061samples 5 mm in thickness, 10 mm in width and 100 mm in length using a Gen III High-Pressure Portable Cold Spray System manufactured by VRC Metal Systems at the Kostas Research Institute (KRI) for Homeland Security of Northeastern University. The sieved Al2024 and Al6061 powders had an average hardness of HV109 and HV75, respectively, determined on cross sections of 10 to 15 particles under 98.07 mN with a dwell time of 15 s using a SHIMADZU HMV-2T micro-Vickers hardness tester. Two CS Al6061 strips were sprayed, one with helium gas (hereafter Al6061-He) and the other with nitrogen gas (hereafter Al6061-N_2). One Al2024 strip was deposited with helium gas (hereafter Al2024-He). Table I summarizes the CS conditions used to spray the Al2024 and Al6061 strips, including the average particle impact velocities determined with the Oseir HiWatch HR system for the three samples, and the critical velocities of the Al2024 and Al6061 powders calculated with a semi-empirical equation[6] for the impact conditions computed with a quasi-one-dimensional analytical cold spray process mode.[34]

B. *Post-CS Deformation Processing*

1. *Rolling*

The Al2024-He and Al6061-He strips, removed from the substrate, were rolled longitudinally at 100 °C (373 K) in 2 passes for total thickness reductions of 40 and 50 pct for Al6061-He and 40 and 55 pct for Al2024-He. To minimize bending during rolling, the Al2024-He and Al6061-He strips were sandwiched between 1-mm-thick steel sheets. Al6061-N_2 could not be rolled without cracking due to its insufficient interparticle bonding.

2. *Ultrasonic ironing*

In lieu of rolling, the Al6061-N_2 strip was subjected to ultrasonic ironing (UI), illustrated in Figure 1, to 'iron out' the residual porosity in the deposit and make the material more metallurgically intact. UI was tested in this work based on the known effect of ultrasonic vibration to enhance the plastic deformation of metals through rapid dislocation unpinning[35–37] which would boost dynamic recovery and recrystallization.[36] The UI experiments were done at 200 °C and 300 °C (473 K and 573 K) under a uniaxial pressure of 100 MPa for a fixed vibration time of 6 seconds at vibration frequency of 20 kHz and an amplitude of 9 μm. As UI does not require removal of CS material from the substrate, it may provide an alternative method of post-CS deformation processing for CS materials that cannot be removed from the substrate for rolling, as is the case in on-site repair. In this work, UI was tested only on Al6061-N_2 removed from the substrate which could not be rolled without cracking.

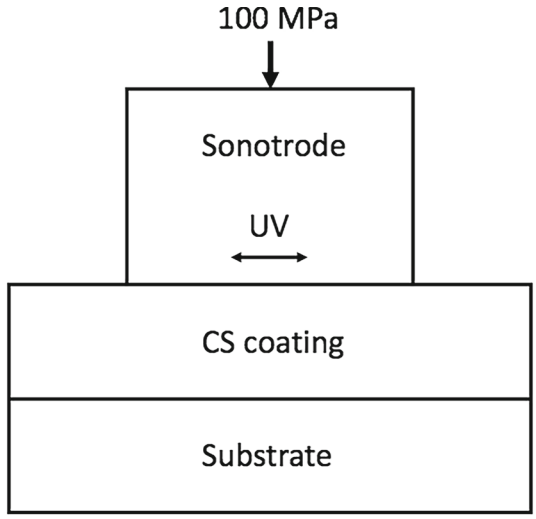

Fig. 1—Schematic illustration of ultrasonic ironing (UI). CS coating either kept on or removed from substrate can be subjected to ultrasonic vibration. In this work the CS coating was removed from the substrate. A sonotrode with a 4 mm × 4 mm square tip was used.

C. *Ultrasonic Washing Test (UWT)*

The interparticle bonding of the CS samples was assessed by an ultrasonic washing test (UWT) in which polished transverse cross sections of the samples were subjected to ultrasonic waves in water to cause weakly bonded particles to come off, leaving voids on the sample surface, Figure 2.[31] The areal percentage of the voids left by detached particles was determined by image analysis on binary micrographs transformed using ImageJ.[38] The percentage of particle retention (hereafter pct particle retention), defined as 100 pct minus the

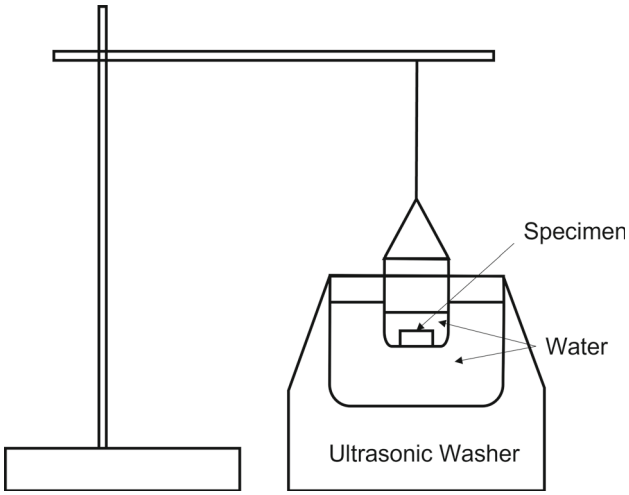

Fig. 2—Schematic illustration of UWT setup.[31].

areal percentage of surface voids, was determined for washing times up to 100 minutes at two levels of washing power, 80 and 120 W, using a Fisher Scientific F20D Ultrasonic Cleaner and a DK Sonic Ultrasonic Cleaner (3L), respectively. The value of pct particle retention at each increment of washing time was calculated by averaging the values determined in 4 to 5 areas on the polished surface at the middle of the specimen thickness. UWT data were analyzed with respect to CS process parameters (stock powder average hardness and spraying gas), washing power and post-CS deformation conditions (thickness reduction in rolling and UI temperature).

D. *Tensile Tests*

The Al6061-He and Al2024-He materials were tensile-tested at room temperature in the as-sprayed state, T6 temper without rolling and T6 temper after rolling. Standard T6 heat treatments were applied; solutionizing at 530 °C (803 K) for 1 hours and water quench to room temperature, followed by artificial aging at 175 °C (448 K) for 8 hours for Al6061-He, and 495 °C (768 K) for 1 hours and water quench, followed by artificial aging at 195 °C (468 K) for 12 hours for Al2024-He. ASTM E8/E8M-16 standard-size tensile specimens,[39] 3.5 mm in thickness, 6 mm in width, and 25 mm in gauge length, were machined in the longitudinal direction of sprayed strips and tested on an Instron 5582 100 kN Universal Tensile Electromechanical tester at an initial strain rate of 0.00033 s^{-1}.

E. *Metallographic Characterization*

Polished CS Al specimens subjected to UWT were examined under an Olympus VANOX-T optical microscope for surface voids left behind by detached particles. The bonding among deposited particles was investigated by TEM/STEM. Lamella specimens for TEM/STEM were fabricated parallel to the transverse cross section of deposited strips by focused ion beam (FIB) using the FEI Scios DualBeam^{TM} FIB at the KRI. TEM/STEM imaging of the FIB lamellae was done with the FEI Titan Themis 300 S/TEM, also at KRI.

III. RESULTS AND DISCUSSION

A. *Ultrasonic Washing Test (UWT)*

Figure 3 shows optical micrographs of a polished transverse cross section of an Al6061-N_2 specimen at 5, 25 and 100 minutes of UWT at 80 W. The dark spots in the images are surface voids created when loosely bonded particles came off the polished cross section during UWT. The continuous increase of particle detachment with washing time indicates weak interparticle bonding in the N_2-sprayed specimen.

1. *Effect of spraying gas*

Figure 4 shows the pct particle retentions of as-sprayed Al6061-N_2 and Al6061-He over 100 minutes of UWT at 80 W. At time zero, no appreciable voids were detected on either specimen, indicating that both materials had achieved virtually full density during CS. However, the pct particle retention of Al6061-N_2 decreased at an overall rate of 0.15 pct per minute, which attests that the deposited particles in the N_2-sprayed material were not bonded well. It should be noted that the deposition efficiency of Al6061-N_2, determined by mass measurement, was only 33 pct, reflecting the subcritical particle impact velocity (721 m/s) at which this material was deposited. Thus, spraying with nitrogen gas suffers from both low deposition efficiency and poor bonding of deposited particles. This also suggests that sprayed particles remained deposited only because they acquired partial bonding that was sufficient to prevent them from bouncing off at impact. In contrast, the Al6061-He material exhibited a nearly zero particle detachment rate. Thus, spraying with helium gas increased interparticle bonding as well as deposition efficiency which was virtually 100 pct as expected for the supercritical mean impact velocity (1075 m/s). However, the Al6061-He material still lost some particles during UWT (see also Figure 6), which attests that the particles in the He-sprayed material were not completely bonded metallurgically.

2. *Effect of UWT power*

Figure 5 compares the particle retentions of Al6061-N_2 at ultrasonic washing powers of 80 and 120 W. At 80 W, the pct particle retention decreased almost linearly with washing time to 85 pct over 100 minutes. At 120 W, the pct particle retention decreased even faster to 74 pct over 100 minutes, with an initial rapid drop of about 7.5 pct during the first 5 minutes and 18 pct over the first 25 minutes. The observations that more particles came off at 120 W than at 80 W and that particle detachment never stopped over the 100 minutes at either washing power attest that the particles in Al6061-N_2 had only partial metallurgical bonding, augmented weakly by mechanical interlocking.

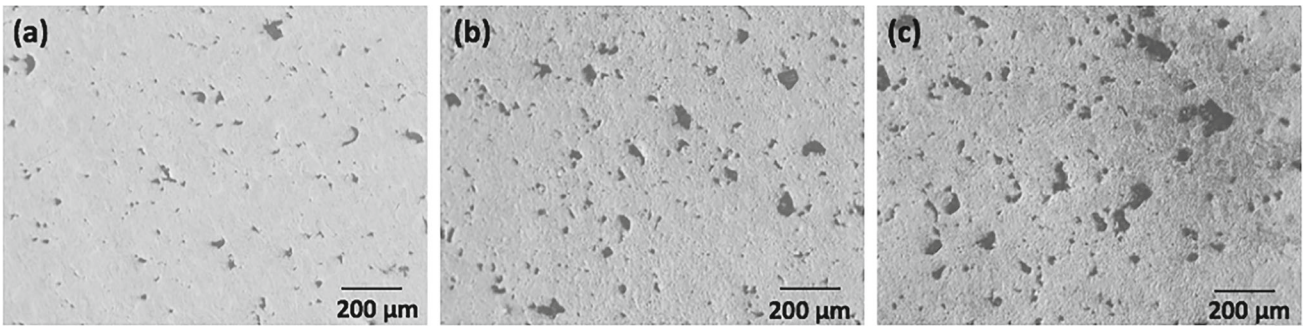

Fig. 3—Optical micrographs of an Al6061-N_2 specimen subjected to UWT at 80 W for (*a*) 5 minutes, (*b*) 25 min and (*c*) 100 min.

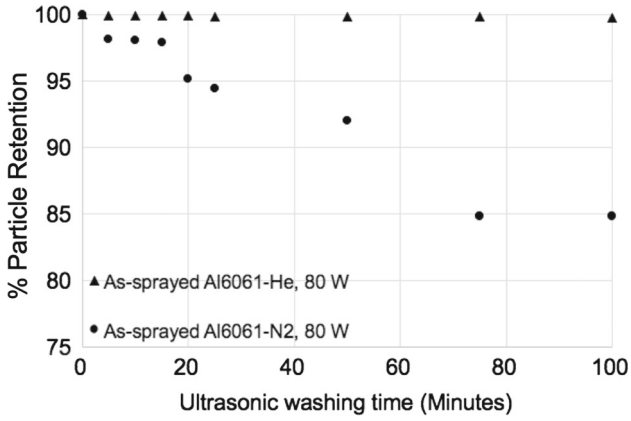

Fig. 4—Ultrasonic washing time *vs* pct particle retention of Al6061-He and Al6061-N_2. UWT at 80 W. Standard deviations range between 0.002 and 0.012 pct.

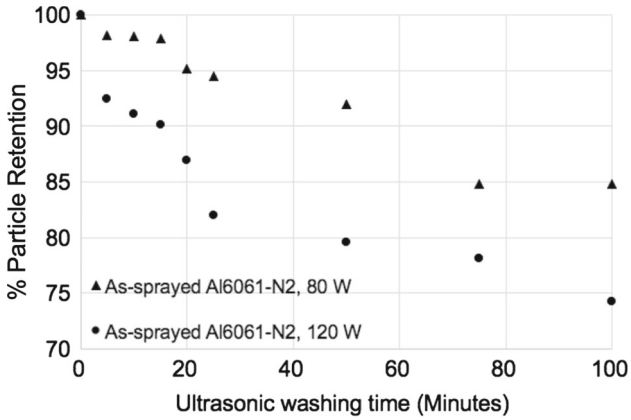

Fig. 5—Ultrasonic washing time *vs* pct particle retention of Al6061-N_2. UWT at 80 W and 120 W. Standard deviations range between 0.001 and 0.011 pct.

Since mechanical interlocking is much weaker than metallurgical bonding,[40] the relative contributions of metallurgical bonding and mechanical interlocking may be assessed from (1) the difference in pct particle retention between 80 and 120 W and (2) the rate of decrease in pct particle retention with UWT time. A

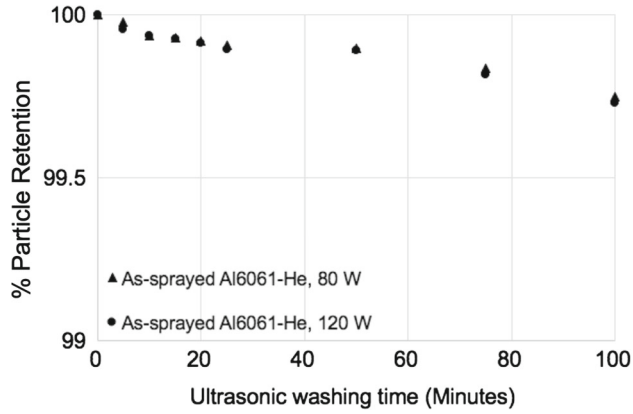

Fig. 6—Ultrasonic washing time *vs* pct particle retention of Al6061-He at 80 W and 120 W. Standard deviations range between 0.001 and 0.012 pct.

large difference in pct particle retention between 80 and 120 W and a high rate of reduction of pct particle retention, *i.e.*, the slope of the plot, translate into a low contribution of metallurgical bonding. The latter was the case with the Al6061-N_2 material for which the average particle detachment rates were 0.15 pct per minute at 80 W and 0.26 pct per minute at 120 W. Moreover, the large initial drop of pct particle retention observed at 120 W indicates that the Al6061-N_2 material contained particles that were bonded more loosely with less metallurgical bonding than the rest, *i.e.*, not all particles were bonded at the same strength.

Al6061-He kept much higher pct particle retentions during UWT, Figure 6, which decreased only slightly to about 99.75 pct over 100 minutes with virtually no dependence on the washing power. Thus, most of the particles in Al6061-He had a higher level of metallurgical bonding than those in Al6061-N_2. However, as mentioned earlier, the low, but non-zero particle detachment rates attest that metallurgical bonding was still incomplete in Al6061-He as well. In fact, even a zero particle detachment rate does not necessarily translate into full metallurgical bonding. It only guarantees that particles are bonded to the extent that is sufficient for them to survive UWT at the power applied.

3. *Effect of powder hardness*

An important factor that may affect the interparticle bonding of CS Al alloys is the hardness of powder particles[41,42] as it relates to the extent of plastic deformation of depositing powder particles required for the formation of metallurgical bonding at particle-substrate and particle-particle interfaces.[28] Figure 7 shows this effect for Al6061-He and Al2024-He which were created with an Al6061 powder (average hardness HV75) and an Al2024 powder (average hardness HV109), respectively. Although both materials kept most (> 99.6 pct) particles over 100 minutes of UWT, the pct particle retention of Al2024-He showed a rapid drop during the initial 20 minutes, followed by a nearly constant trend, while that of Al6061-He decreased only slowly at a nearly constant rate of 0.0025 pct/min with no appreciable initial drop. The initial drop of pct particle retention of Al2024-He indicates that a small fraction of the particles of the Al2024-He material had distinctly weaker bonding, *i.e.*, less metallurgical bonding, than the rest and hence would come off more readily. The absence of an initial drop in pct particle retention and the low particle detachment rate of Al6061-He indicate that particles of the Al6061 material were bonded more uniformly and at a higher level of metallurgical bonding which would keep most of the deposited particles on the sample during the UWT at 80 W.

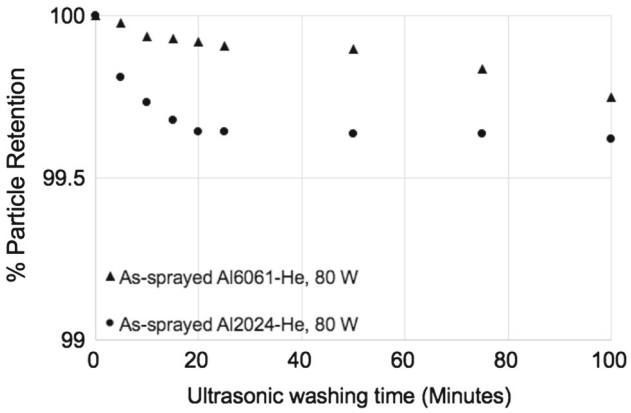

Fig. 7—Ultrasonic washing time *vs* pct particle retention of Al6061-He and Al2024-He created with soft Al6061 powder (HV75) and harder Al2024 powder (HV109). UWT at 80 W. Standard deviations range between 0.002 and 0.040 pct.

4. *Effect of rolling*

Figure 8(a) shows pct particle retention vs. UWT time at 120 W for an as-sprayed Al6061-He specimen and two Al6061-He specimens, each rolled at 100 °C (373 K) in two passes, one for a total thickness reduction of 40 pct and the other for 50 pct. While the as-sprayed Al6061-He specimen lost particles at a rate of about 0.0025 pct per minute, the rolled specimens both exhibited a lower particle detachment rate of about 0.001 pct per minute indicative of increased metallurgical bonding in the rolled specimens. However, the low but finite detachment rates indicate that the metallurgical bonding of the particles was still partial in the rolled materials.

Figure 8(b) shows pct particle retention vs. UWT time at 120 W for an as-sprayed Al2024-He specimen and two Al2024-He specimens, each rolled at 100 °C (373 K) in two passes for total thickness reductions of 40 and 55 pct. As also observed at 80 W, Figure 7, the as-sprayed Al2024-He exhibited a quick drop in pct particle retention during the initial 15 minutes, followed by a lower particle detachment rate of about 0.001 pct per minute. This suggests that some (~ 0.04 pct) of the particles in the as-sprayed specimen had distinctly weaker metallurgical bonding than the rest. The 40 pct-rolled specimen also exhibited a similar initial drop, indicating that rolling 40 pct was not enough to entirely prevent the loose particles from coming off. The 55 pct-rolled sample, however, showed no initial drop. Thus, rolling 55 pct effectively increased the bonding of the loose particles in the as-sprayed material. After about 50 minutes of UWT, the three samples all showed similar low particle detachment rates of about 0.001 pct per minute. Thus, rolling decreased the particle

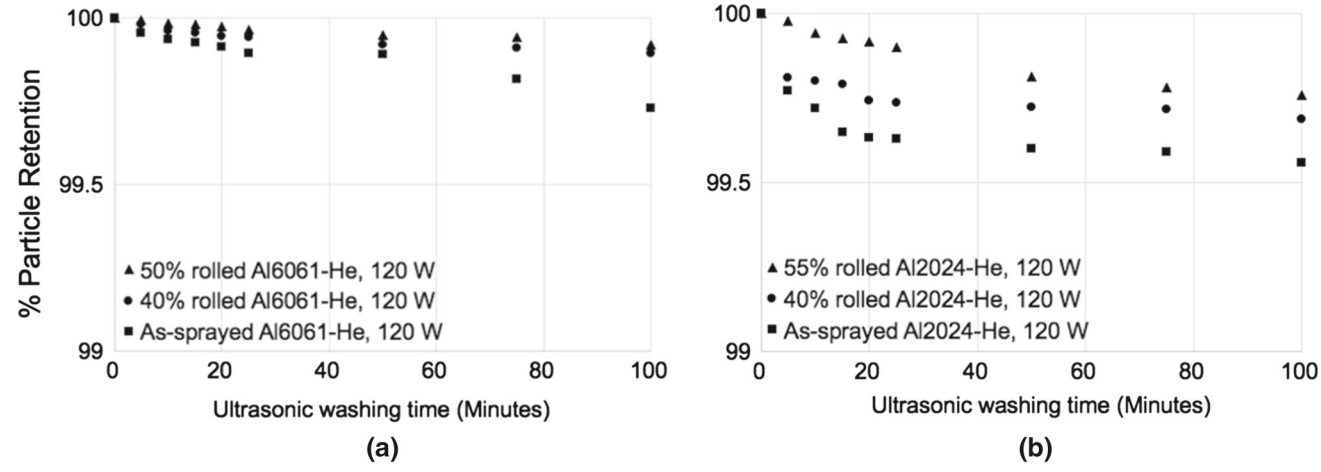

Fig. 8—Effect of rolling at 100 °C (373 K) on pct particle retention during UWT at 120 W: (*a*) Al6061-He, (*b*) Al2024-He. Standard deviations in (a) and (b) range between 0.001 and 0.010 pct and 0.003 and 0.053 pct, respectively.

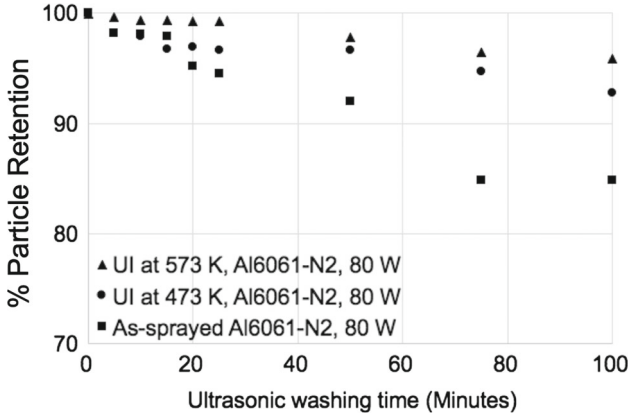

Fig. 9—Effect of UI at 200 °C and 300 °C (473 K and 573 K) on the particle retention of Al6061-N_2 during UWT at 80 W. UI time was fixed at 6 s. Standard deviations range between 0.004 and 0.011 pct for as-sprayed Al6061-N_2 and 0.006 and 2.37 pct for UI-processed Al6061-N_2 specimens.

detachment of Al2024-He mainly by increasing the metallurgical bonding of loose particles that existed in the as-sprayed material.

5. *Effect of ultrasonic ironing (UI)*

Ultrasonic ironing (UI), as an alternative means of post-CS deformation processing, was tested on Al6061-N_2 which would crack when rolled because of its poor interparticle bonding. Figure 9 compares pct particle retentions during UWT for specimens subjected to UI at 200 °C and 300 °C (473 K and 573 K) for 6 seconds with the UWT data of as-sprayed Al6061-N_2 from Figure 4. While the as-sprayed specimen lost 15 pct of the surface particles over the 100 minutes of UWT, the specimen subjected to UI at 200 °C (473 K) lost 7 pct and the specimen subjected to UI at 300 °C (573 K) lost even less (4 pct) surface particles. Thus, UI increased the interparticle bonding in Al6061-N_2 significantly. However, the particle detachment rates of the UI-processed Al6061-N_2 specimens are still 40 to 75 times higher than those of the rolled Al6061-He, indicating that UI, within the conditions applied to Al6061-N_2, did not increase the interparticle bonding of Al6061-N_2 to a level comparable to that of rolled Al6061-He. Moreover, as indicated in the figure captions, the pct particle retention values of the UI-processed specimens are associated with higher standard deviations than those of the rolled specimens. This indicates that UI, as applied in the manner shown in Figure 2 using a small sonotrode with a 5 mm × 5 mm square tip, did not produce as uniform an effect as rolling. Nonetheless, the present results are encouraging as commercial production of structural CS materials would require low-cost N_2 spaying which produces weakly bonded materials that are not adaptable to rolling.

B. *Tensile Tests*

Figure 10 shows the stress-strain curves of as-sprayed, T6 heat-treated, and 40 pct rolled and T6 heat-treated

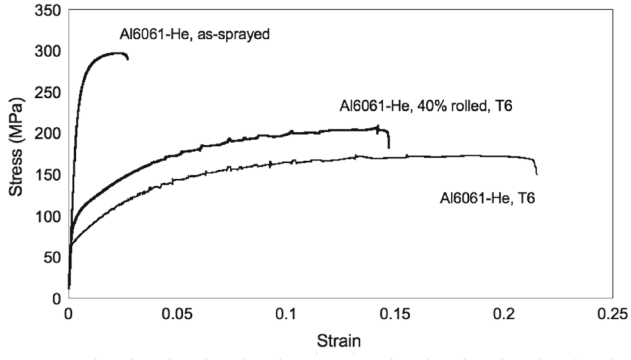

Fig. 10—Stress–strain curves of as-sprayed, T6 heat-treated and rolled and T6 heat-treated Al6061-He specimens.

specimens of Al6061-He machined in the longitudinal direction of the deposited strip. The flow stress of the as-sprayed specimen reached an ultimate tensile strength (UTS) of 300 MPa, while the elongation was low at 2.5 pct, both reflecting the severely strained microstructure from CS[28] (see also Figure 13(a)). The low tensile ductility should also reflect the incomplete metallurgical bonding of the as-sprayed Al6061-He material as revealed by UWT, Figures 6, 7 and 8(a). T6 heat treatment drastically increased the elongation to 22 pct, while also decreasing the yield strength to 70 MPa and the UTS to 170 MPa. The improved ductility reflects increased interparticle bonding as well as softening caused by the T6 heat treatment. Previous studies also showed this effect of post-CS heat treatment.[43,44] The rolled and T6 heat-treated specimen showed a somewhat lower elongation (14 pct) at a higher yield strength (90 MPa) and UTS (200 MPa), indicative of finer grains produced by recrystallization during the T6 heat treatment after rolling.

The strength values of the T6 heat-treated and rolled and T6 heat-treated Al6061-He specimens, however, are lower than the values reported for wrought Al6061-T6 (yield strength: 276 MPa).[45,46] This discrepancy indicates that neither of the T6 treated and rolled and T6 treated Al6061-He materials possessed full interparticle bonding, which would limit both flow stress and strain hardening rate. The serrated stress-strain curves of these specimens also reflect the incomplete interparticle bonding in these materials. The stress-strain curve of the as-sprayed specimen does not exhibit serrations because the specimen fractured prematurely before serrations would show up.

Figure 11 shows the stress-strain curves of as-sprayed, T6 heat-treated, and 40 pct rolled and T6 heat-treated specimens of Al2024-He that were machined in the longitudinal direction of the deposited strip. The high flow stress of the as-sprayed specimen reaching 380 MPa at fracture reflects the strain-hardened microstructure from CS, while the low elongation (~ 2 pct) also indicates a low level of interparticle bonding in this as-sprayed material as well, despite its high pct particle retention in UWT (95.6 pct at 100 minutes), Figure 8(b). As was the case with the Al6061-He specimen, T6 heat treatment (495 °C (768 K) for

1 hours, water quench, 195 °C (468 K) for 12 hours) drastically increased the elongation to 11 pct, while also decreasing the flow stress at fracture to 325 MPa. The rolled and T6 heat-treated specimen also showed an 11 pct elongation but at a higher flow stress reaching 370 MPa, which reflects a combined effect of warm rolling and T6 heat-treatment. However, both the T6 heat-treated and rolled and T6 heat-treated Al2024-He specimens exhibited discontinuous-like yielding followed by serrated stress-strain curves, which indicates that neither specimen achieved complete metallurgical interparticle bonding.

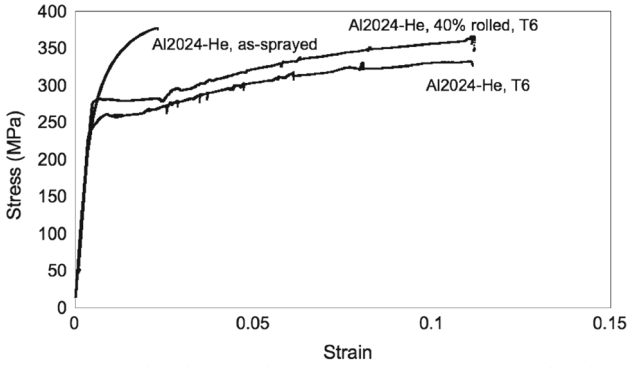

Fig. 11—Stress–strain curves of standard-size specimens of as-sprayed, T6 heat-treated and rolled and T6 heat-treated Al2024-He specimens.

Figure 12 shows the fracture surfaces of the as-sprayed and 40 pct rolled and T6 heat-treated Al6061-He and Al2024-He tensile specimens. The as-sprayed Al6061-He and Al2024-He specimens, Figures 12(a) and (c), both exhibit crevices and facets that occurred along their particle boundaries, which attest that the poor bonding at the particle boundaries was primarily responsible for the low tensile ductility of the as-sprayed materials. Such crevices and facets indicative of interparticle fracture were less frequent and much smaller and shallower in the fracture surfaces of the rolled and T6 treated specimens, Figures 12(b) and (d), indicating increased interparticle bonding in these materials. Consequently, the fracture of the rolled and T6 treated Al2024 and Al6061 specimens occurred mainly through the particles, leaving fine dimples in the trans-particle fracture regions Figures 12(b) and (d).

The above tensile test results are consistent with the UWT results which indicated increased, but still partial interparticle bonding in the rolled and T6 treated Al6061-He and Al2024-He materials.

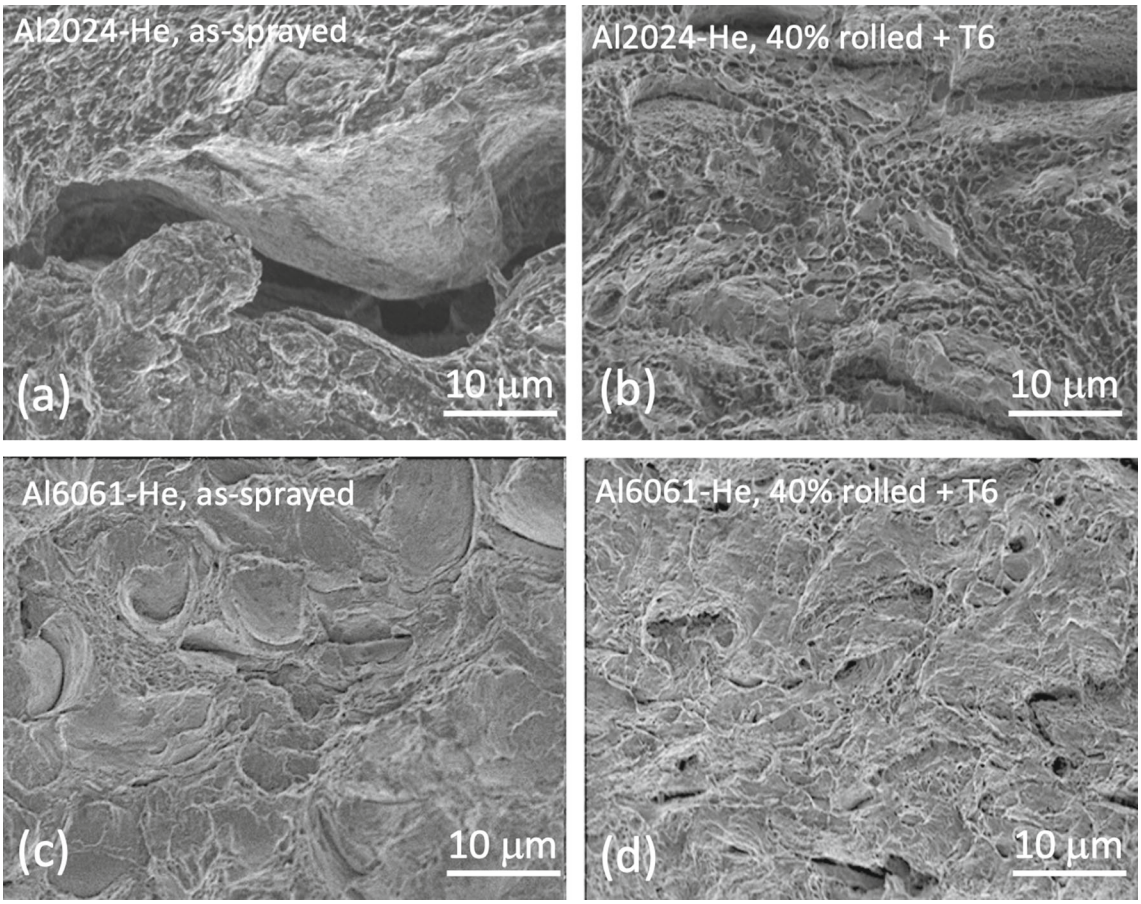

Fig. 12—Fracture surfaces of tensile specimens of Al2024-He and Al6061-He. (*a*) As-sprayed Al2024, (*b*) 40 pct -rolled and T6 heat-treated Al2024, (*c*) as-sprayed Al6061, (*d*) 40 pct -rolled and T6 heat-treated Al6061.

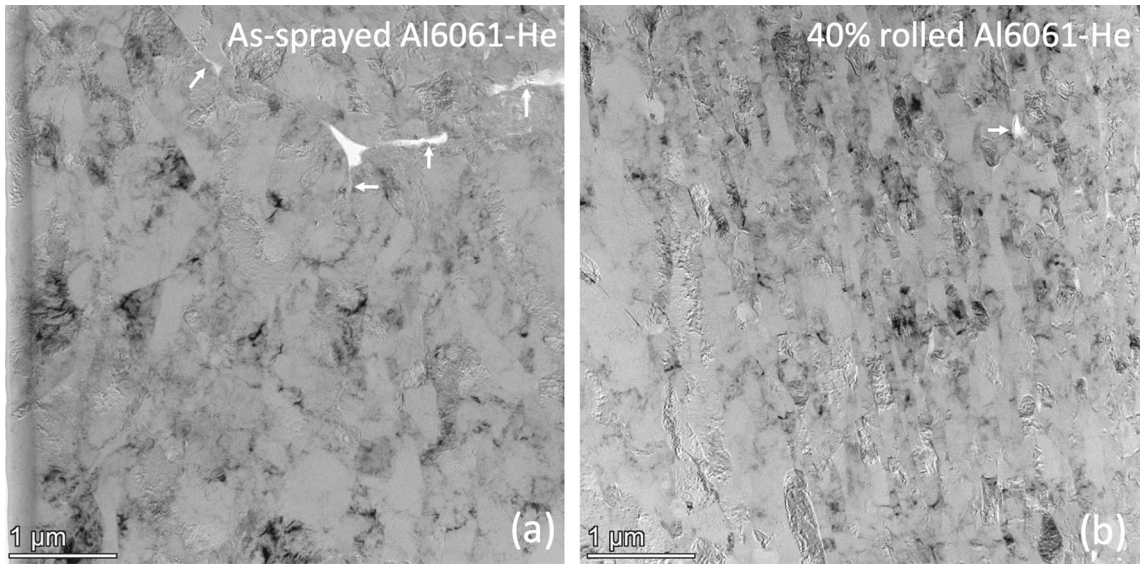

Fig. 13—Low-magnification TEM images of (*a*) as-sprayed Al6061-He. Particle boundaries are not totally metallurgically bonded (arrows). (*b*) 40 pct rolled Al6061-He showing residual porosity (arrow).

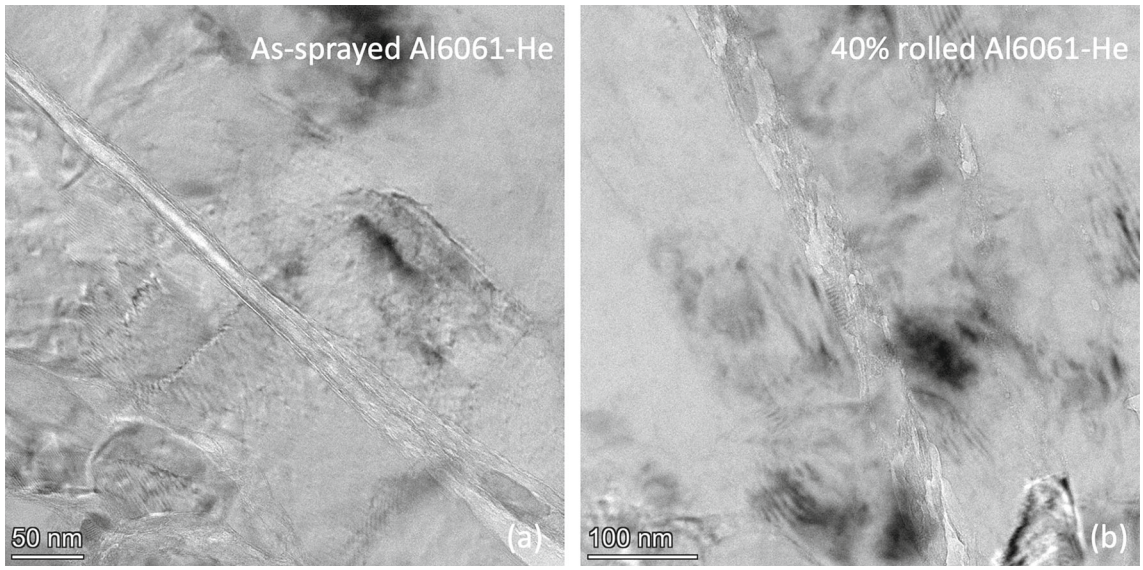

Fig. 14—Oxide layers at particle boundaries inherited from Al6061 powder particles. (*a*) a continuous oxide layer at a particle boundary in as-sprayed Al6061-He, (*b*) a sheared oxide layer in 40 pct rolled Al6061-He allowing for partial metallurgical bonding through channels of sheared oxide layer.

C. *TEM/STEM Characterization*

Figure 13 shows TEM micrographs of the as-sprayed and 40 pct rolled Al6061-He specimens. The as-sprayed specimen, Figure 13(a), shows cellular grains in particles, about 1 μm in diameter, inherited from gas atomization, but with evidence of severe deformation and dynamic recovery from CS.[28] The grains in the rolled specimens, Figure 13(b), are finer and elongated, reflecting the deformation and dynamic recrystallization caused by warm rolling at 100 °C (373 K).

The as-sprayed specimen shows an opening at a triple particle junction. Thus, full density was not strictly achieved even by He-spraying, despite the virtually full density assessed by image analysis for this specimen. Moreover, the particle boundaries extending from the triple junction appear to lack good bonding (arrows). The rolled specimen, Figure 13(b), also exhibits a small opening at a particle boundary (arrow) despite the significant thickness reduction (40 pct) in rolling.

Although the rest of the particle boundaries in Figures 13(a) and (b) appear bonded, examining at higher magnification reveals that these particle boundaries are associated with oxide layers, Figure 14. Oxide layers along particle boundaries commonly occur in CS aluminum alloys as depositing powder particles all come with tenacious surface oxide.[28,47] The surface oxide of

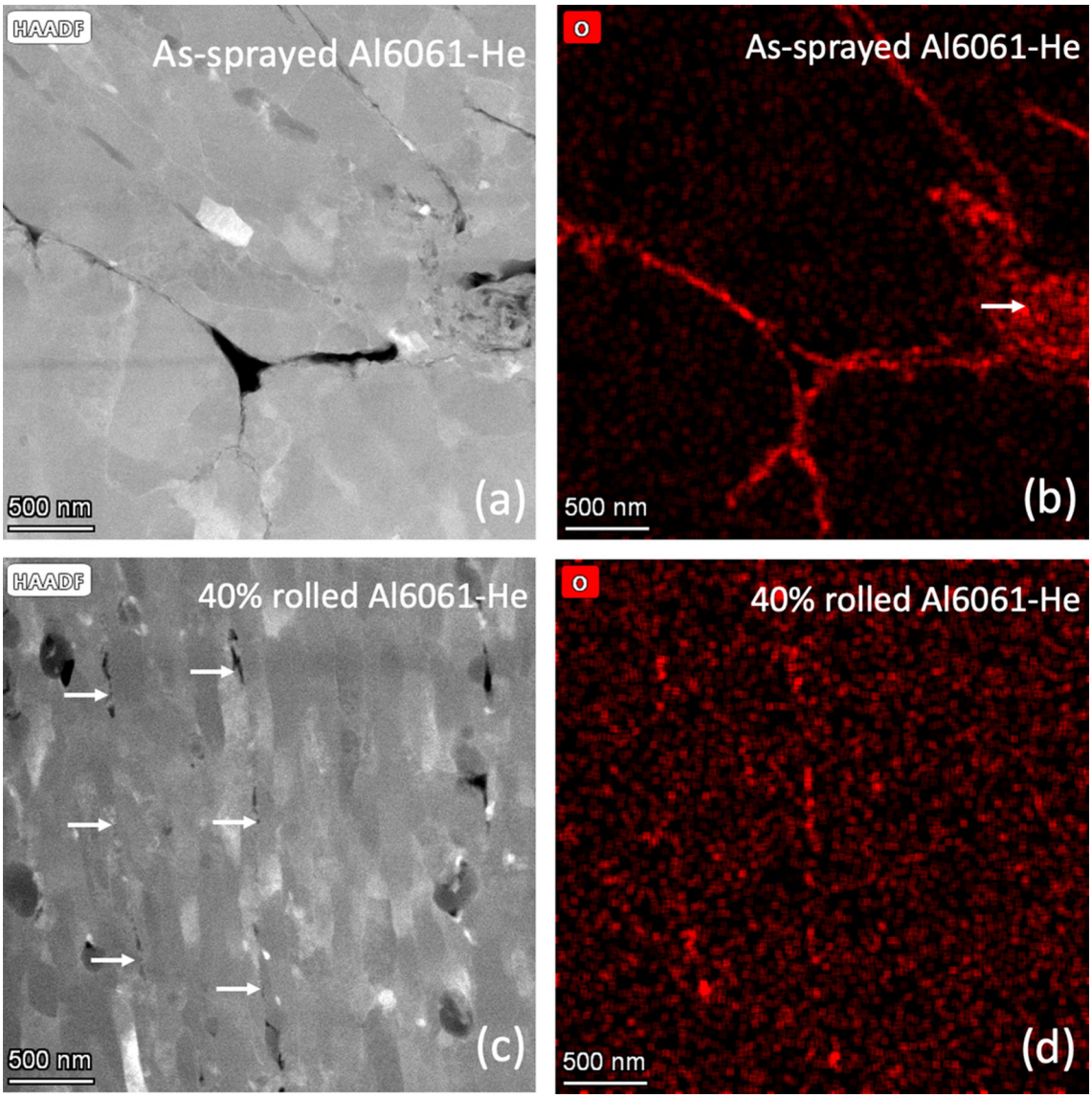

Fig. 15—HAADF images and EDS oxygen mappings. (*a*) and (*b*) as-sprayed Al6061-He, (*c*) and (*d*) 40 pct rolled Al6061-He.

aluminum alloy powders, which forms during gas atomization, is preferred as it prevents pyrophoric explosion during gas atomization and storage. Consequently, the oxide layer in the as-sprayed sample is highly continuous, Figure 14(a), and as such would act to restrict metal-to-metal joining or metallurgical bonding.[28] Most particle boundaries in the as-sprayed Al6061-He specimen in fact had highly continuous oxide layers. In contrast, the oxide layers in the rolled specimen are sheared into small pieces, Figure 14(b), which would allow for partial metallurgical bonding through the channels of the oxide fragments.

Figures 15(a) and (b) shows a high-angle annular dark-field (HAADF) image and an EDS oxygen mapping of the as-sprayed Al6061-He specimen at the triple particle junction region in Figure 13(a). The oxygen mapping confirms the presence of nearly continuous oxide layers along the particle boundaries of the as-sprayed material. One of the particle boundaries, oriented nearly normal to the electron beam, Figure 15(b) (arrow), shows its 'side view' in which the oxide layer is seen fragmented into fine pieces. However, the oxide fragments remain at the particle boundary in high density and as such would limit metallurgical bonding to a low level. Another notable feature of importance in Figure 15(b) is at the unfilled triple junction where the edges of the three particles are trimmed with an oxide layer. This suggests that every depositing particle of Al powder came with its own surface oxide layer, producing particle boundaries with double oxide layers, as also confirmed in Figure 14(a).

The particle boundaries in the rolled Al6061-He specimen, Figures 15(c) and (d), also exhibit oxide at particle boundaries, but at a higher degree of fragmentation. The observation that the particle boundaries in Figure 15(c) (arrows) are parallel to the elongated grains suggests that these particle boundaries were stretched in the rolling direction, providing larger oxide-free areas

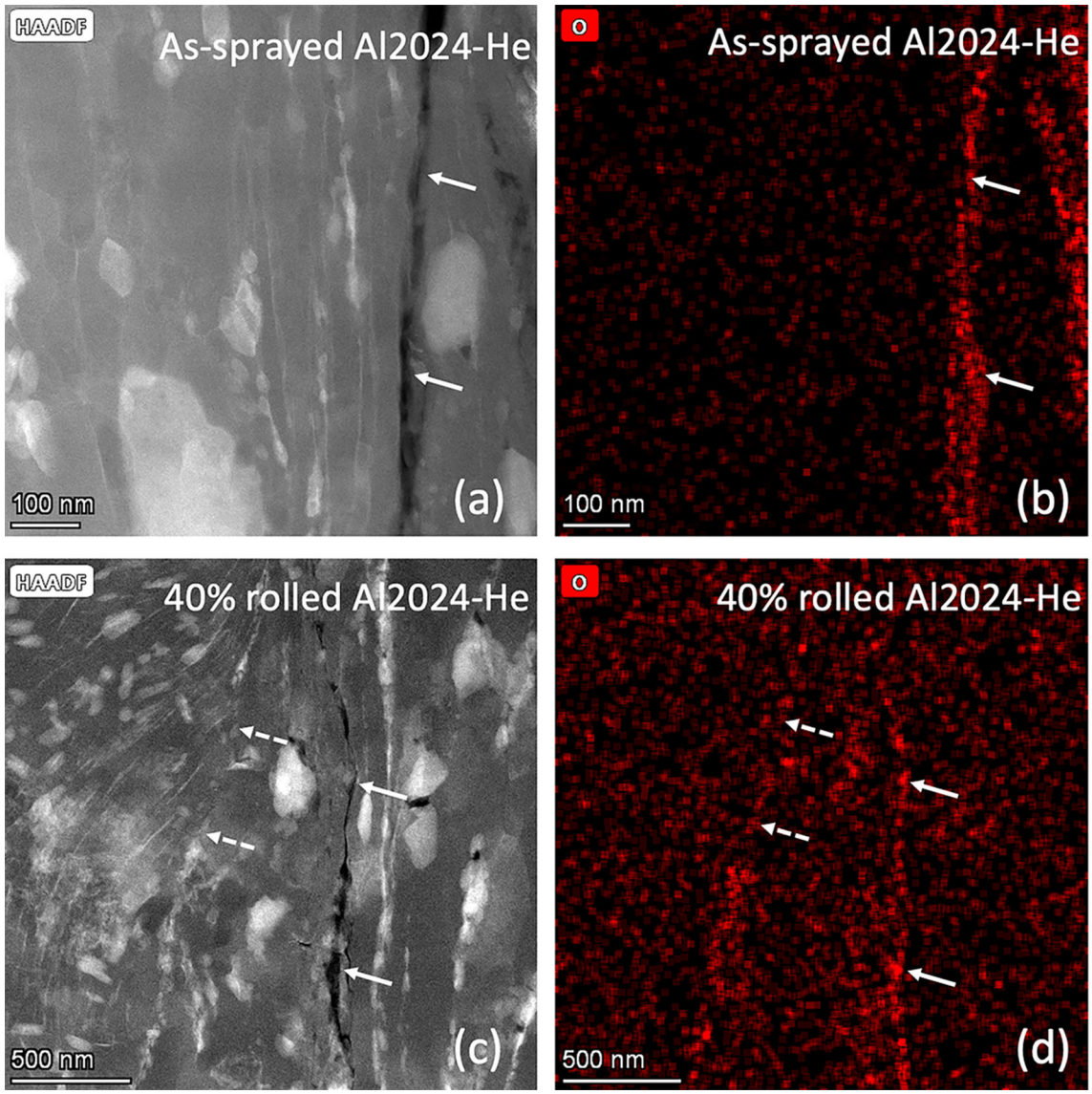

Fig. 16—HAADF image and EDS oxygen mapping of particle boundaries in Al2024-He. (*a*) and (*b*) as-sprayed specimen, (*c*) and (*d*) 40 pct rolled specimen. Solid arrows indicate unbonded particle boundaries. Dashed arrows show a bonded particle boundary in the rolled specimen.

for metallurgical bonding, Figure 15(d). However, since rolling never really eliminates the oxide at the particle boundaries, the metallurgical (metal-to-metal) bonding at the closed particle boundaries in a rolled material would still be partial to the extent that depends on the amount of deformation by rolling.

Figure 16 shows HAADF images and EDS oxygen mappings of the as-sprayed and rolled Al2024-He specimens. Particle boundaries that are obviously not bonded are seen in both specimens (solid arrows). Thus, rolling 40 pct did not bond all particle boundaries in Al2024-He either. Such unbonded particle boundaries may be found especially with the loose particles that caused the initial drop of pct particle retentions of the as-sprayed and 40 pct rolled Al2024-He in Figures 7 and 8(b). As is the case with Al6061-He, the unbonded particle boundaries in the Al2024-He specimens are also characterized by layers of densely populated oxide particles, Figures 16(b) and (d), which restrict metallurgical bonding. However, many of the particle boundaries in the rolled specimen, such as the one pointed to with dashed arrows, are completely closed with much lower oxide density and thus are metallurgically bonded to a higher degree, Figures 16(c) and (d).

Fragmented oxide layers at particle boundaries were observed in an Al6061-N_2 specimen subjected to ultrasonic ironing (UI) at 573 K for 6 seconds as well, Figure 17 (arrows). Thus, the increased particle retention of the specimen, Figure 9, also is considered to result from oxide fragmentation at particle boundaries caused by UI. Although more work is required to determine the extent to which UI can increase the interparticle bonding in CS aluminum alloys, post-CS UI has the potential to improve the mechanical integrity of CS aluminum alloy parts to which rolling does not apply.

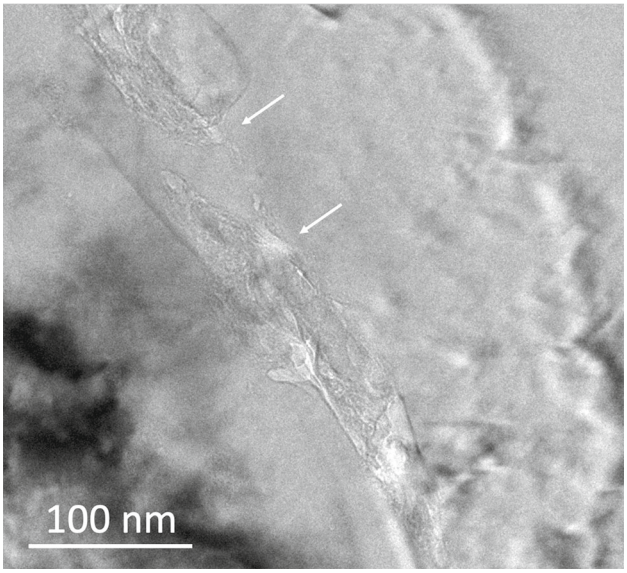

Fig. 17—Fragmented oxide at a particle boundary in Al6061-N_2 subjected to ultrasonic ironing at 300 °C (573 K) for 6 s.

In summary, particle boundaries in as-sprayed Al6061 and Al2024 materials are associated with highly continuous layers of oxide which restrict the metallurgical bonding of deposited particles as evidenced by the low particle retention and tensile ductility of the as-sprayed materials. Post-CS deformation processing, by warm rolling or UI, provides an effective means of increasing the mechanical integrity of CS aluminum alloys through fragmenting and dispersing the oxide at particle boundaries.

IV. CONCLUSIONS

The interparticle bonding and ductility of CS Al2024 and Al6061 were assessed by ultrasonic washing tests (UWT) and tensile tests, and the effects of post-CS warm rolling and ultrasonic ironing (UI) on interparticle bonding were characterized by TEM and STEM. The major findings are:

1. UWT provides an effective means for the semi-quantitative assessment of interparticle bonding in cold sprayed aluminum alloys.
2. Spraying with a lighter gas, *e.g.*, helium gas, and a softer powder, Al6061 in this work, produces stronger interparticle bonding in the deposited material.
3. As-cold sprayed Al6064 and Al2024 do not possess complete interparticle metallurgical (metal-to-metal) bonding, as reflected by their low tensile ductility.
4. A nearly 100 pct deposition efficiency, achieved at a supercritical impact velocity, does not necessarily translate into full interparticle metallurgical bonding. Sprayed particles remain in the deposit only because they acquire partial bonding at the impact that is sufficient to prevent them from bouncing off.
5. Particle boundaries in cold sprayed Al6064 and Al2024 are associated with highly continuous layers of oxide inherited from original powder which restrict the metallurgical bonding at the particle boundaries and hence limit the ductility of the CS aluminum alloys.
6. Post-CS warm rolling is effective in increasing the interparticle bonding and hence ductility of CS Al alloys. Rolled CS Al alloys in T6 temper exhibited elongations comparable to those of wrought counterparts, but at lower strengths indicative of still incomplete interparticle bonding as manifested by serrated stress-strain curves of the material.
7. The improved interparticle bonding and ductility of rolled CS Al alloys arise from fragmentation of inherent oxide layers and a consequent increase in metallurgical (metal-to-metal) joining at the particle boundaries. Post-CS ultrasonic ironing also produces similar effects on interparticle bonding.

ACKNOWLEDGMENTS

The authors thank Tricia Schwartz, Samuel Boese and Jay Sanchez at the Kostas Research Institute of Northeastern University for their technical support in preparing cold sprayed samples, Wentao Liang, also at the Kostas Research Institute, for his assistance in the TEM/STEM work, and Scott Julien at Northeastern University for his help with tensile tests. This research was sponsored by the Army Research Laboratory and was accomplished under Cooperative Agreement Number W911NF-20-2-0024. The views and conclusions contained in this document are those of the authors and should not be interpreted as representing the official policies, either expressed or implied, of the Army Research Laboratory or the U.S. Government. The U.S. Government is authorized to reproduce and distribute reprints for Government purposes notwithstanding any copyright notation herein.

FUNDING

Open access funding provided by Northeastern University Library.

CONFLICT OF INTEREST

The authors declare that they have no conflict of interest.

OPEN ACCESS

REFERENCES

1. F. Gärtner, T. Stoltenhoff, T. Smidt, and H. Kreye: *J. Therm. Spray Technol.*, 2006, vol. 15(2), pp. 223–32.
2. H. Assadi, F. Gartner, T. Stoltenhoff, and H. Kreye: *Acta Mater.*, 2003, vol. 51, pp. 4379–94.
3. V.K. Champagne: *The Cold Spray Materials Deposition Process: Fundamentals and Applications*, Woodhead Publishing, Cambridge, 2007, pp. 1–7.
4. A. Mordi, S. Hassani-Gangaraj, M. Guangliano, and M. Dao: *Surf. Eng.*, 2014, vol. 30(6), pp. 369–95.
5. W.B. Choi, L. Li, V. Luzin, R. Neiser, T. Gnaupel-Herold, H.J. Prask, S. Sampath, and A. Gouldstone: *Acta Mater.*, 2007, vol. 55, pp. 85–66.
6. T. Schmidt, H. Assadi, F. Gartner, H. Ritcher, T. Stoltenhoff, H. Kreye, and T. Kiassen: *J. Therm. Spray Technol.*, 2009, vol. 18(5–6), pp. 794–808.
7. W. Wong, E. Irissou, A.N. Ryabinin, J.-G. Legoux, and S. Yue: *J. Therm. Spray Technol.*, 2011, vol. 20(1–2), pp. 213–16.
8. M. Fukumoto, H. Terada, M. Mashiko, K. Sato, M. Yamada, and E. Yamaguchi: *Mater. Trans.*, 2009, vol. 50(6), pp. 1482–88.
9. F. Chen, F. Li, Q. Shen, and L. Zhang: *J. Phys. Conf. Ser.*, 2006, vol. 419(1), p. 012006.
10. P.C. King, A.J. Poole, S. Horne, R. de Nys, S. Gulizia, and M.Z. Jahedi: *Surf. Coat. Technol.*, 2013, vol. 216, pp. 60–67.
11. H. Che, P. Vo, and S. Yue: *Surf. Coat. Technol.*, 2017, vol. 313, pp. 236–47.
12. D. Zhang, P.H. Shipway, and D.G. McCartney: *J. Therm. Spray Technol.*, 2005, vol. 14(1), pp. 109–16.
13. K. Ko, J. Choi, and H. Lee: *Mater. Lett.*, 2016, vol. 175(15), pp. 13–15.
14. H. Singh, T.S. Sidhu, S.B.S. Kalsi, and J. Karthikeyan: *J. Braz. Soc. Mech. Sci. Eng.*, 2013, vol. 35(3), pp. 231–45.
15. J. Villafuerte and D. Wright: *Adv. Mater. Proc.*, 2010, vol. 168(5), pp. 53–55.
16. P. Cavaliere and A. Silvello: *J. Therm. Spray Technol.*, 2017, vol. 26(4), pp. 661–70.
17. C.A. Widener, M.J. Carter, O.C. Ozdemir, R.H. Hrabe, B. Hoiland, T.E. Stamey, V.K. Champagne, and T.J. Eden: *J. Therm. Spray Technol.*, 2016, vol. 25(1–2), pp. 193–201.
18. A. Sova, S. Grigoriev, A. Okunkova, and I. Smurov: *Int. J. Adv. Manuf. Technol.*, 2013, vol. 69(9–12), pp. 2269–78.
19. J. Pattison, S. Clotto, R. Morgan, M. Bray, and W. O'Neill: *Int. J. Mach. Tools Manuf.*, 2007, vol. 47(3–4), pp. 627–34.
20. Y. Cormier, P. Dupuis, and B. Jodoin: *J. Therm. Spray Technol.*, 2013, vol. 22(7), pp. 1210–21.
21. S. Pathak and G.C. Saha: *Coatings*, 2017, vol. 7(8), pp. 122–49.
22. G. Prasher and H. Vasudev: *J. Clean. Prod.*, 2021, vol. 310, p. 127606. https://doi.org/10.1016/j.jclepro.2021.127606.
23. S. Yin, P. Cavaliere, B. Aldwell, R. Jenkins, H. Liao, W. Li, and R. Lupoi: *Add. Manuf.*, 2018, vol. 21, pp. 628–50.
24. M. Rokni, C. Widener, and V.K. Champagne: *J. Therm. Spray Technol.*, 2014, vol. 23(3), pp. 514–24.
25. M. Rokni, C. Widener, and G. Crawford: *Surf. Coat. Technol.*, 2014, vol. 251, pp. 254–63.
26. M. Rokni, C. Widener, G. Crawford, and M.K. West: *Mater. Sci. Eng. A*, 2015, vol. 625, pp. 19–27.
27. Y. Zou, W. Qin, E. Irissou, J.-G. Legoux, S. Yue, and J.A. Szpunar: *Scr. Mater.*, 2009, vol. 61(9), pp. 899–902.
28. W.C. Evans, X. Dan, A. Houshmand, S. Müftü, and T. Ando: *Metall. Mater. Trans. A*, 2019, vol. 50A, pp. 3937–48.
29. T. Van Steenkiste and J.R. Smith: *J. Therm. Spray Technol.*, 2004, vol. 13(2), pp. 274–82.
30. S.H. Zahiri, D. Fraser, S. Gulizia, and M. Jehedi: *J. Therm. Spray Technol.*, 2006, vol. 15(3), pp. 422–30.
31. Y. Li, Y. Hamada, K. Otobe, and T. Ando: *J. Therm. Spray Technol.*, 2016, vol. 26(3), pp. 350–59.
32. P. Nautiyal, C. Zhang, V.K. Champagne, B. Boesl, and A. Agarwal: *Mater. Sci. Eng. A*, 2018, vol. 737, pp. 297–308.
33. M. Grujicic, C.L. Zhaoa, C. Tonga, W.S. DeRosset, and D. Helfritch: *Mater. Sci. Eng. A*, 2014, vol. 368, pp. 222–30.
34. O.Ç. Özdemir, J.M. Conahan, and S. Müftü: *Coatings*, 2020, vol. 10(12), p. 1254.
35. B. Langenecker: *IEEE Trans. Sonics Ultrason.*, 1966, vol. 13, pp. 1–8.
36. H. Huang and T. Ando: *Metall. Mater. Trans. A*, 2022, vol. 53A, pp. 2797–2810.
37. T. Ando and A. Houshmand: *Materialia*, 2019, vol. 8, p. 100472.
38. C.A. Schneider, W.S. Rasband, and K.W. Eliceiri: *Nat. Methods*, 2012, vol. 9, pp. 671–75.
39. W. Conshohocken: *ASTM E8/E8M-16a Standard Test Methods for Tension Testing of Metallic Materials*, vol. 3, ASTM International, West Conshohocken, 2016, pp. 3–4.
40. T. Hussain, D.G. McCartney, P.H. Shipway, and D. Zhang: *J. Therm. Spray Technol.*, 2009, vol. 18(3), pp. 364–79.
41. X. Dan: MS thesis, Northeastern University, 2020.
42. B. Jodoin, L. Ajdelsztajn, E. Sansoucy, A. Zúñiga, P. Richer, and E. Lavernia: *Surf. Coat. Technol.*, 2006, vol. 201(6), pp. 3422–29.
43. R. Sinclair-Adamson, M. Harbidge, and R. Murray: *J. Therm. Spray Technol.*, 2021, vol. 30(10), pp. 1493–1511.
44. K. Ito and K. Ogawa: *J. Therm. Spray Technol.*, 2014, vol. 23(1–2), pp. 104–113.
45. J.R. Davis, P. Allen, S. Lampman, T.B. Zorc, S.D. Henry, J.L. Daquila and A.W. Ronke: *Metals Handbook: Properties and Selection: Nonferrous Alloys and Special-Purpose Materials,* ASM International 10th Ed., 2, 1990, p. 404.
46. H.E. Boyer and T.L. Gall: *Heat Treating of Non-ferrous Alloys, Metals Handbook*, American Society for Metals, Materials Park, 1985, pp. 1030–39.
47. D. Zhang, P.H. Shipway, and D.G. McCartney: *J. Therm. Spray Technol.*, 2005, vol. 14, pp. 10–16.